ELSEVIER

International Journal of Heat and Fluid Flow 23 (2002) 398–412

International Journal of HEAT AND FLUID FLOW

www.elsevier.com/locate/ijhff

LES of unsteady turbulence via a one-equation subgrid-scale transport model

Anne Dejoan [1], Roland Schiestel *

Institut de Recherche sur les Phénomènes Hors Equilibre, IRPHE, UMR 6594 CNRS/Universités d'Aix-Marseille I & II, 49, rue Frédéric Joliot Curie, BP 146 13384 Marseille Cedex 13, France

Received 15 July 2000; accepted 1 February 2002

Abstract

The study of unsteady turbulent flows can lead to non-equilibrium turbulence spectra and there is a need to develop new subgrid-scale models that can be efficient in such situations. This is particularly necessary if the grid is coarse and the cutoff lies before the inertial zone of the spectrum. The model should be able to behave like a standard LES when the filter is sharp and like RANS models when the filter is wide, in a progressive way. The present work is a first step in that direction made by using transport equations for the subgrid-scale turbulence. We have used a transposition of the statistical model of Hassid and Poreh. The results of the simulations show that the one-equation model can predict the lag effects in the turbulent field response in pulsed channel flow, while the usual Smagorinsky model fails in several aspects.

Keywords: Large eddy simulation; Turbulence; Unsteady flow; Spectral non-equilibrium; Subgrid-scale model

1. Introduction

Unsteady turbulent flows prevail in a wide variety of situations occurring in industrial or environmental applications. Unsteady turbulence still needs new modelling and simulation tools with enough generality to tackle the problem of non-equilibrium turbulence that results in non-standard spectral distributions of the turbulent energy. Just cite for instance the important hysteresis occurrences in aeronautical situations.

We consider here the unsteadiness created by periodic forcing in turbulent plane channel flow by means of imposed periodic oscillations of the mean longitudinal pressure gradient. This pulsed turbulent channel flow has been thoroughly investigated experimentally by Binder and Kueny (1981) and Tardu et al. (1994) who have studied the effect of various frequency and amplitude regimes of the imposed perturbation on the turbulent flow field. The particular choice of this specific turbulent flow is well suited to illustrate non-equilibrium turbulence because it represents an example of complex flow that can be studied numerically in a relatively simple way. First, there is only one non-homogeneous direction (normal to the walls) and second, the time periodicity of the forcing allows the use of a phase averaging procedure which gives a detailed description of the turbulent field response.

The experimental results have put in light lag effects that, in particular, appear between the modulation of the Reynolds stresses and the mean axial velocity. These effects have been also evidenced by Hanjalic and Stosic (1983) using full turbulence closure. In the case of large eddy simulations, this non-equilibrium behaviour cannot be reproduced by using a subgrid-scale model as simple as the classical Smagorinsky model, which is based on an implicit equilibrium hypothesis. More advanced models have been proposed in the literature including the dynamic model proposed by Germano et al. (1991) and the structure model of Metais and Lesieur (1992). Transport equations of the subgrid-scale turbulence have also been introduced by Horiuti and Yoshizawa (1986), Schumann (1975) and also Deardorff (1973). This latter approach is an appealing route for developing a hybrid method that bridges the LES

* Corresponding author. Tel.: +33-04-96139765; fax: +33-04-96139709.

E-mail address: schieste@irphe.univ-mrs.fr (R. Schiestel).

[1] Present address: ICMCB, 87 avenue du Dr. A. Schweitzer, 33608 Pessac, France.

0142-727X/02/$ - see front matter
PII: S0142-727X(02)00144-3

approach and the RANS approach. In the present paper, we propose a first step in this direction, using a one-equation transport model to calculate the subgrid turbulence field. It is also a first step to get rid of equilibrium or similarity hypothesis that impedes models derived from the Smagorinsky concept.

In the first part of the present paper, the proposed modelling method developed to study the pulsed channel flow is presented. It includes the phase averaging statistical procedure, the filtering approach and the numerical method. Particular attention is focussed on the derivation of the one-equation subgrid-scale model, which differs from the Horiuti and Yoshizawa (1986) or Schumann (1975) models in several aspects. In the second part, the Smagorinsky model and the transport equation model predictions are compared in the case of fully turbulent steady channel flow. This allows to validate the transport equation model formulation, indeed for this peculiar quasi-equilibrium flow, both models should lead to an equivalent behaviour. The third part is dedicated to the discussion of the predictions obtained in the oscillatory flow for each type of model. The influence of the density of mesh points is also considered.

2. Numerical approach and models

2.1. Term decomposition

The analysis is based on a formalism using a four-term decomposition. Each instantaneous variable q is split into a statistical mean value and a fluctuating part. The statistical mean value is in fact identified as the phase average and can be in its turn, split into a time mean value $\langle q\rangle$ and a phase periodic oscillation $\tilde{q}$. The fluctuating turbulent part is then composed of an explicit part q'_{exp} simulated by the numeric and an implicit part q'_{imp}, which is modelled

$$q = \langle q\rangle + \tilde{q} + q'_{\mathrm{exp}} + q'_{\mathrm{imp}} \tag{1}$$

After a filtering operation applied on the instantaneous Navier–Stokes equations and modelling the subgrid-scale turbulent stresses using a subgrid-scale viscosity hypothesis, we obtain the following well-known equations of motion for LES

$$\begin{aligned} &\frac{\partial \overline{U}_i}{\partial t} + \frac{\partial \overline{\overline{U}_i \overline{U}_j}}{\partial x_j} = F_i - \frac{1}{\rho}\frac{\partial \overline{\pi}}{\partial x_i} - \frac{\partial \boldsymbol{\tau}_{ij}}{\partial x_j} + \frac{1}{Re_\tau}\nabla^2 \overline{U}_i \\ &\frac{\partial \overline{U}_i}{\partial x_i} = 0 \end{aligned} \tag{2}$$

with $\overline{U} = \langle U\rangle + \tilde{U} + U'_{\mathrm{exp}}$ and in which Re_τ denotes the Reynolds number defined as $Re_\tau = u_\tau \delta/\nu$, while $F_i = ((\partial\pi/\rho)/\partial x)\delta_{i1}$ is the mean gross pressure gradient necessary to maintain the motion and $\boldsymbol{\tau}_{ij}$ is the subgrid-scale stress tensor. The pressure $\overline{\pi}$ is referred to as "pseudo-pressure" because it includes the spherical part of the stress tensor.

All the quantities are non-dimensionalized using the wall shear velocity u_τ and the half-width δ of the channel. The present computations use a Gaussian filter in the two periodic directions x and y, which produces a progressive and smooth transition between resolved and unresolved scales. Generally, the filter width Δ_i is chosen twice the mesh spacing h_i in the direction (i) (c.f. Kwak et al., 1975). In the z inhomogeneous direction, the filter is produced by the grid discretisation.

The response of the flow to the forcing is picked out by extracting the organised part of the unsteady motion using phase averaging (see decomposition (1)) in which the phase is given by the imposed periodic driving force. This statistical procedure is used in the experiments (Tardu and Binder, 1993; Tardu et al., 1994) and has also been applied to the non-filtered Navier–Stokes equations by Reynolds and Hussain, 1972 in their theoretical work on unsteady turbulence. The phase average corresponds indeed to the true statistical average.

2.2. Modelling

If we consider the turbulent energy spectrum, the previously described lag effects will appear, in terms of spectra, as a departure from the universal equilibrium Kolmogoroff spectrum. This effect has to be included in the subgrid-scale modelling approach. The subgrid-scale model behaviour will of course depends on the location of the cut-off induced by the filter which lies between the two extreme limits that are the complete direct numerical simulation (DNS) in which all the turbulent scales are resolved and the model is not active, and the one point statistical modelling in which all the turbulent scales are modelled. Reasoning in spectral space, when the filter cut-off κ_c goes to infinity, the calculation must approach a DNS, whereas in the case of a vanishing cut-off, the calculation must in principle approach full statistical modelling.

As it has been yet mentioned above, both the Smagorinsky and a one-equation subgrid-scale models are explored in the present large eddy simulations applied to the pulsed turbulent channel flow. These models are both based on the subgrid-scale viscosity hypothesis, and thus the stress tensor $\boldsymbol{\tau}_{ij}$ takes the form

$$\boldsymbol{\tau}_{ij} = -2\nu_{\mathrm{sgs}}\overline{S}_{ij} \quad \text{with} \quad S_{ij} = \frac{1}{2}\left(\frac{\partial \overline{U}_i}{\partial x_j} + \frac{\partial \overline{U}_j}{\partial x_i}\right) \tag{3}$$

where ν_{sgs} denotes the subgrid-scale turbulence viscosity defined from characteristic length and velocity scales. The two models make use of the subgrid length scale l_{sgs} linked to the mesh size used in the calculation and defined as

$$l_{\mathrm{sgs}} = [\Pi \min(\Delta_m, l^*)]^{1/3} \tag{4}$$

with $l^* = 0.1\delta/C_s$ for $z \leqslant 0.1\delta/\kappa$ and $l^* = \kappa z/C_s$ for $z \leqslant 0.1\delta/\kappa$, where Δ_m denotes the filter width in the (m) direction, δ the width of the shear layer, z the wall distance and $\kappa = 0.41$ the Karman constant. Then, in the case of a very coarse mesh, l_{sgs} is limited by the classical mixing length in full statistical modelling.

The relevant difference between the Smagorinsky model and the transport model results from the subgrid-scale viscosity formulation. For the Smagorinsky model the velocity scale is directly linked to the instantaneous filtered deformation tensor

$$v_{sgs} = (C_s l)^2 \sqrt{2\overline{S}_{ij}\overline{S}_{ij}} \quad \text{for} \quad z \geqslant z_C \tag{5a}$$

$$v_{sgs} = C_2 \frac{l^4}{v}(2\overline{S}_{ij}\overline{S}_{ij}) \quad \text{for} \quad z \leqslant z_C \tag{5b}$$

with $C_s = 0.2$, $C_2 = C_s^2/27\kappa$.

The relation (5b) expresses the effects of molecular viscosity in the low Reynolds number near wall regions. The quantity z_C represents the distance to the wall for which the two subgrid-scale viscosities (5a) and (5b) once averaged on horizontal planes are equal.

In the case of the one-equation model the subgrid velocity scale is given by the kinetic turbulent energy of the implicit turbulent field k_{sgs} and hence

$$v_{sgs} = C_{vsgs} l_{sgs} k_{sgs}^{1/2} \tag{6}$$

The closure of the subgrid-scale turbulent kinetic energy transport equation is inspired from the Hassid and Poreh model (1975) in which the near wall viscous effects are accounted for by coefficients that are functions of the turbulence Reynolds number.

Transposing this full statistical closure to the case of subgrid modelling leads to the following proposed equation:

$$\frac{\partial k_{sgs}}{\partial t} + \overline{U}_j \frac{\partial k_{sgs}}{\partial x_j} = -\tau_{ij}\frac{\partial \overline{U}_i}{\partial x_j} D_{sgs} - \varepsilon_{sgs} \tag{7}$$

In order to include the viscous effects, the expression for v_{sgs} is converted into:

$$v_{sgs} = C_{vsgs} l_{sgs} k_{sgs}^{1/2}\left[1 - \exp(-A_{vsgs} R_{sgs})\right]$$

and the kinetic energy dissipation rate is given by

$$\varepsilon_{sgs} = C_{\varepsilon sgs}\frac{k_{sgs}^{3/2}}{l_{sgs}}\left[\frac{2}{C_{\varepsilon sgs} R_{sgs}} + 1 - \exp(-A_{vsgs} R_{sgs})\right] \tag{8}$$

with $R_{sgs} = (l_{sgs} k_{sgs}^{1/2})/v$, the Reynolds number defined on the subgrid-scale.

A gradient diffusion hypothesis is used for the kinetic energy:

$$D_{sgs} = \frac{\partial}{\partial x_j}\left(v + \frac{v_{sgs}}{\sigma_{sgs}}\frac{\partial k_{sgs}}{\partial x_j}\right) \tag{9}$$

The original Hassid and Poreh model is exactly recovered when the spatial resolution becomes very coarse and full statistical modelling is approached. This practice is justified by considering the statistical model as the upper limit that should reach the one-equation model when the filter size is very large. In such a case (when κ_c vanishes, see Fig. 1) the average kinetic energy of the implicit turbulent scales approaches the overall turbulence energy of the flow. However, the numerical constants appearing in the above equations have to be valid for any filter size. These constants have been determined and controlled in the case of a classical quasi-equilibrium turbulent channel flow used as a reference case and using the Smagorinsky model. The following values are retained (see Appendix A):

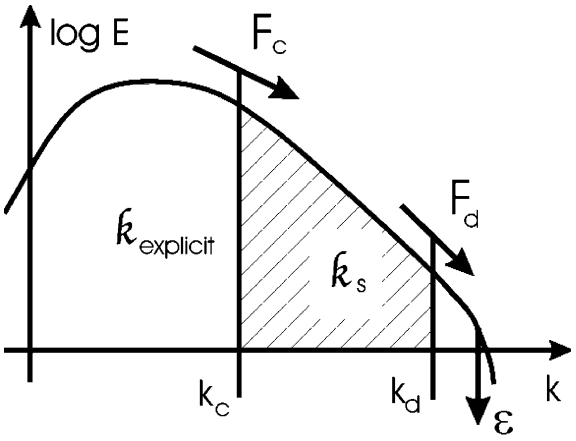

Fig. 1. Partioning of the energy spectrum for large eddy simulation.

$$C_{vsgs} = 0.116, \quad C_{\varepsilon sgs} = 0.85,$$
$$A_{vsgs} = 0.229 \quad \text{and} \quad \sigma_{sgs} = 1$$

In the case of steady turbulent channel flow, the Smagorinsky and the one-equation model should behave similarly since no appreciable departure from equilibrium occurs and the Kolmogorov hypothesis prevails. On the contrary, when the flow is submitted to forced oscillations, the behaviour of the models should differ. Having in mind the energy spectrum partitioning sketched in Fig. 1, the Smagorinsky model implicitly assumes that the dissipation ε_{sgs} varies continuously in compliance with the large scales of the flow field governed by the production process. In pulsed flow, this implies that the implicit turbulent field varies in phase with the forcing, hence no lag or history effect can be accounted for. On the contrary, the transport equation model, through its partial kinetic energy equation, allows an account of time delay effects between the subgrid-scale motion and the forced oscillation imposed on the mean flow. The dissipation term (Eq. (8)) only expresses that the characteristic dissipation scale of subgrid turbulence is connected to the characteristic subgrid length scale and not at all to the large scales. Thus, the modelled scales are thereby not directly influenced by the large energy

containing eddies, but only by the energy flux $F_c = -\tau_{ij}(\partial\overline{U}_i/\partial x_j)$ through the cut-off (Fig. 1).

2.3. Numerical method

The numerical method for solving the instantaneous flow field is based on Hermitian fourth order schemes and pseudo-spectral Fourier developments (Schiestel and Viazzo, 1995 and Viazzo and Schiestel, 1995). The Navier–Stokes equations are solved using the skew-symmetric form of the pressure-velocity formulation on a staggered grid to overcome the pressure checkerboarding problem and to verify good conservation properties for momentum and energy. The time advancement is based on a hybrid Adams-Bashforth and Crank–Nicolson scheme and the pressure-velocity coupling is achieved efficiently by iteratively solving a simplified pressure correction equation.

More precisely, the filtered momentum equations in the skew-symmetric form are

$$\frac{\partial\overline{U}_i}{\partial t} = F_i - \frac{1}{\rho}\frac{\partial\overline{\pi}}{\partial x_i} - \frac{1}{2}\left[\frac{\overline{\partial\overline{U}_i\overline{U}_j}}{\partial x_j} + \overline{U}_j\frac{\partial\overline{U}_i}{\partial x_j}\right] - \frac{\partial\boldsymbol{\tau}_{ij}}{\partial x_j} + \nu\nabla^2\overline{U}_i \tag{10}$$

Fourier pseudo-spectral methods are used in the homogeneous (Ox) and (Oy) directions, whereas the Hermitian finite differences are applied in the inhomogeneous (Oz) direction. In the non-homogeneous direction (Oz) normal to the walls, the mesh is strongly refined near the walls, using the following hyperbolic transformation:

$$z = \frac{1}{a}\tanh[Z\tanh^{-1}(a)] \tag{11}$$

where Z is the uniform coordinate in the transformed space and a an adjustable parameter controlling the refinement. By choosing $N_z = 62$ grid points in the (Oz) direction and $a = 0.98346$, we get three grid points in the viscous layer ($z^+ < 5$). The second order derivative of the Laplacian operator is split into two parts

$$\frac{\partial^2\overline{U}_i^2}{\partial Z^2} = \frac{\overline{U}_{i+1} - 2\overline{U}_i + \overline{U}_{i-1}}{\delta Z^2} + \gamma(\overline{U}_i^2, \partial\overline{U}_i/\partial z) \tag{12}$$

where the first term on the right hand side denotes the second order difference and γ a corrective term to recover fourth order Hermitian finite difference.

We also make use of an averaging process of the eddy viscosity over planes parallel to the walls, giving rise to the decomposition $\nu_{sgs} = \langle\nu_{sgs}\rangle + \nu'_{sgs}$, in which only the terms including $\langle\nu_{sgs}\rangle$ are incorporated in the Crank–Nicolson scheme. All the remaining terms (except the pressure gradient) are inserted in the Adams–Bashforth scheme.

Hence, the discretised equations become:

$$\frac{\overline{U}_i^{n+1} - \overline{U}_i^n}{\Delta t} = \frac{1}{2}(3H_i^n - H_i^{n-1}) - \frac{1}{\rho}\frac{\partial\overline{\pi}^{n+1}}{\partial x_i} + \frac{1}{2}\left(\langle\nu_{sgs}\rangle^n + \nu\right)\delta_{zz}^2(\overline{U}_i^{n+1} + \overline{U}_i^n)$$

$$\frac{\partial\overline{U}_i^{n+1}}{\partial x_i} = 0. \tag{13}$$

(for numerical convenience, the eddy viscosities are evaluated at the previous time step n).

The system (13) is solved using a fractional time step method with an internal iterative process preserving Hermitian accuracy. The initial velocity field in all cases is obtained by interpolation of a previous large eddy simulation carried out for the channel flow at the same Reynolds number with $64 \times 96 \times 62$ grid points (Viazzo, 1993).

For solving the subgrid-scale turbulence equation of the transport model, the hybrid Adams–Bashforth and Crank–Nicolson time scheme has not been retained because of time step limitations due to stiffness of the source terms. So, a different time scheme was introduced for the k_{sgs} equation. The precision loss does not seem a real problem as far as it concerns only the modelled equation.

The discretized form of the k_{sgs} equation is given below

$$\frac{k_{sgs}^{(n)} - k_{sgs}^{(n-1)}}{\Delta t} = P^{(n-1)} - \left(\frac{\varepsilon_{sgs}^{(n-1)}}{k_{sgs}^{(n-1)}}\right)k_{sgs}^{(n)} + \frac{1}{2}\left(\nu + \left\langle\frac{\nu_{sgs}}{\sigma_{sgs}}\right\rangle_{x,y}^{(n-1)}\right)g^2\delta_{zz}^2\left(k_{sgs}^{(n)} + k_{sgs}^{(n-1)}\right) \tag{14}$$

The first term on the right hand side denoted P, contains the advective terms, the production terms and complementary diffusive terms due to variable diffusivity coefficient and non-uniform mesh in the z direction. The spatial derivatives are calculated as previously, using centred Hermitian schemes. This equation can be solved using the tridiagonal algorithm.

The initial conditions are obtained from equilibrium relations deduced from the Smagorinsky model (Appendix A):

$$k_{sgs} = 2\frac{C_{\nu sgs}l_{sgs}^2}{C_{\varepsilon sgs}}\overline{S}_{ij}\overline{S}_{ij}$$
$$\varepsilon_{sgs} = C_{\varepsilon sgs}\frac{k_{sgs}^{3/2}}{l_{sgs}}\left[\frac{2}{C_{\varepsilon sgs}R_{sgs}} + 1 - \exp(-A_{\nu sgs}R_{sgs})\right] \tag{15}$$

3. Preliminary test in fully developed turbulent channel flow

The fully developed turbulent channel flow, characterised by a Reynolds number based on the maximum

mean velocity equal to 13,800 (as in Moin and Kim, 1982), has been chosen as the reference test case of a quasi-equilibrium confined flow. As it has been yet mentioned, the two models considered above ought to give almost identical results in such quasi-equilibrium situation. Thus, this case is helpful for calibrating the subgrid-scale transport equation model.

The discussion turns principally on a direct comparison between the results obtained with the Smagorinsky model and transport equation model for the calculation of steady fully developed channel flow performed on a coarse mesh. However, some grid resolution aspects are included as well and the statistical flow fields computed on a finer mesh with the Smagorinsky model and the one-equation model are compared.

Therefore, two meshes of differing densities have been used in the calculations: a coarse mesh composed of $32 \times 64 \times 62$ points on the domain ($L_x = 2\pi\delta$, $L_y = \pi\delta$, $L_z = 2\delta$) corresponding to the following discrete grid space $\Delta x = 0.19\delta$, $\Delta y = 0.049\delta$, $\Delta z_{\max} = 0.032\delta$, and a fine mesh composed of $256 \times 128 \times 62$ points on the domain ($L_x = 4\pi\delta$, $L_y = 3\pi/2\delta$, $L_z = 2\delta$) corresponding to $\Delta x = 0.049\delta$, $\Delta y = 0.036\delta$, $\Delta z_{\max} = 0.032\delta$. For the fine mesh, the statistically steady state is reached after about a total time of integration $Tu_\tau/\delta = 5$, which represents more than 10 thousands time steps.

The results issued from the simulation of the fully turbulent flow using the Smagorinsky model and the one-equation model are directly compared on Figs. 2–7. The velocity profile as the evolutions along the normal direction to the wall of the turbulent intensity and turbulent shear stress exhibit a similar behaviour for the two models as expected. This is clearly illustrated by the

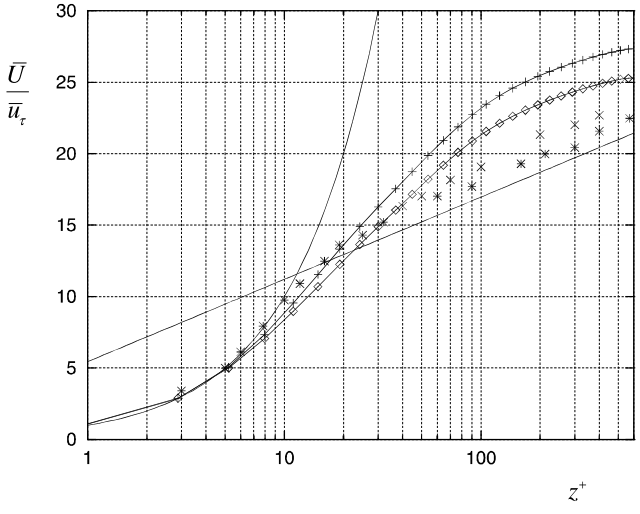

Fig. 2. Mean velocity profiles in fully developed turbulent plane channel flow, (◇) Smagorinsky model ($32 \times 64 \times 62$), (+) one-equation model ($32 \times 64 \times 62$), (−) logarithmic law $2.5\log(z) + 5.45$, (∗) Comte-Bellot experiment (1965, $Re = 57,000$), (×) Laufer experiment (1951, $Re = 12,000$).

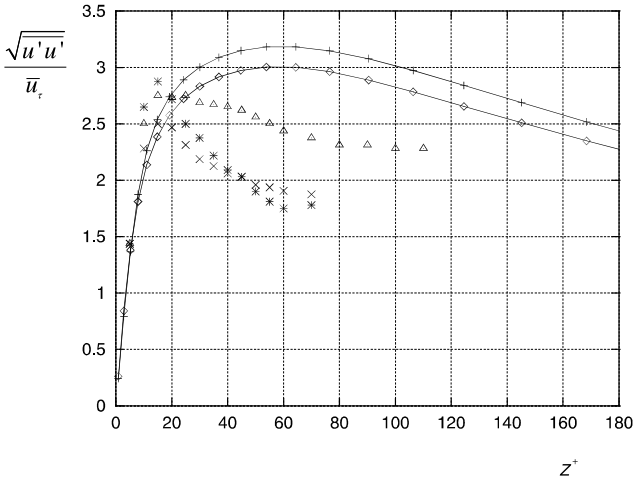

Fig. 3. Mean longitudinal turbulence intensity profiles in fully developed turbulent plane channel flow near the wall, (◇) Smagorinsky model ($32 \times 64 \times 62$), (+) one-equation model ($32 \times 64 \times 62$), (∗) Kreplin and Eckelmann experiment (1979, $Re = 3350$), (×) Hussain and Reynolds experiment (1975, $Re = 13,800$), (Δ) Comte-Bellot experiment (1965, $Re = 64,000$).

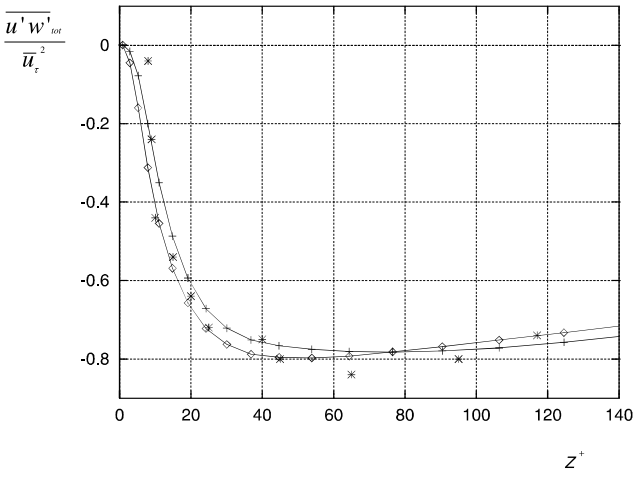

Fig. 4. Total turbulent shear stress profiles in plane channel flow, (◇) Smagorinsky model ($32 \times 64 \times 62$), (+) one-equation model ($32 \times 64 \times 62$), (∗) Wei-Willmarth experiment (1989, $Re = 14,914$).

subgrid-scale turbulence viscosity profile drawn on Fig. 5. The slight quantitative differences observed between the models can result from the description of the near wall region which is not exactly identical for the two models but are still not significant for the purpose of the present paper which is concerned with unsteady turbulence. Such discrepancies between calculations and experiments (velocity and intensity profiles) have been observed in a similar way by Piomelli et al. (1988) in their study on the coupling between the Smagorinsky model and a coarse grid resolution. Refining the mesh provides better agreement with the experiments (Figs. 6,7). However, the simulations of the steady channel flow clearly show that the one transport equation model,

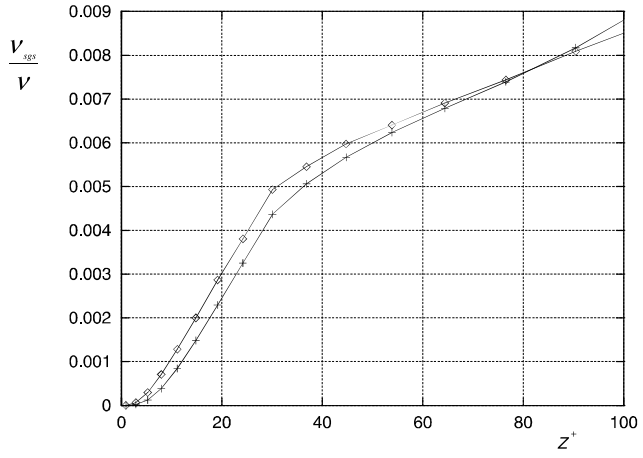

Fig. 5. Subgrid-scale turbulent viscosity (symbols, see Fig. 4).

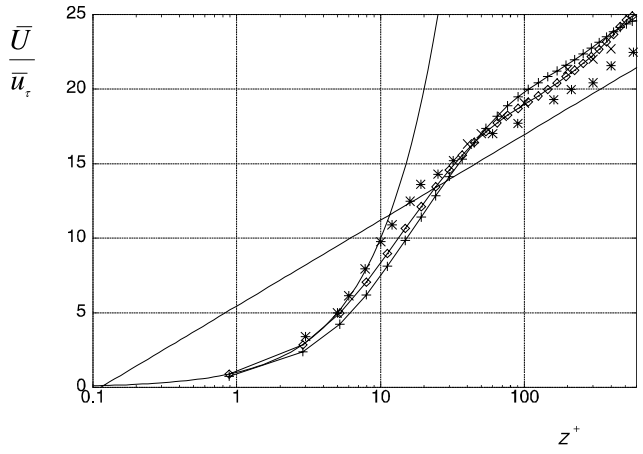

Fig. 6. Mean velocity profiles in fully developed turbulent plane channel flow, (◇) Smagorinsky model ($256 \times 128 \times 62$), (+) one-equation model ($256 \times 128 \times 62$), (−) logarithmic law $2.5\log(z) + 5.45$, (∗) Comte-Bellot experiment (1965, $Re = 57,000$), (×) Laufer experiment (1951, $Re = 12,000$).

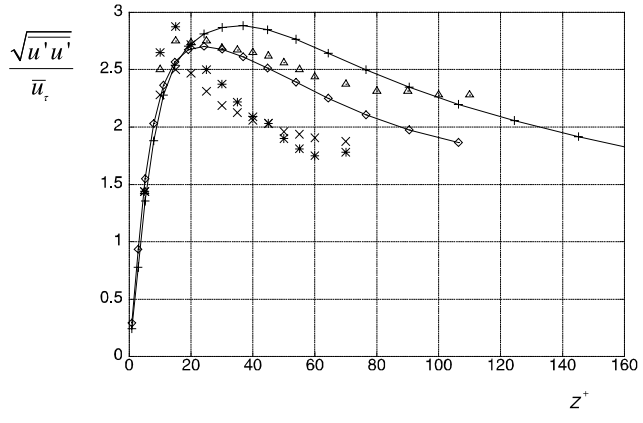

Fig. 7. Mean longitudinal turbulence intensity profiles in fully developed turbulent plane channel flow near the wall, (◇) Smagorinsky model ($256 \times 128 \times 62$), (+) one-equation model ($256 \times 128 \times 62$), (∗) Kreplin and Eckelmann experiment (1979, $Re = 3350$), (×) Hussain and Reynolds experiment (1975, $Re = 13,800$), (Δ) Comte-Bellot experiment (1965, $Re = 64,000$).

at the limit of quasi-equilibrium turbulence, behaves consistently with the widely accepted Smagorinsky model.

4. Turbulent pulsed flow in a plane channel

By superimposing mean velocity oscillations in turbulent channel flow, a modulation of the mean velocity gradient is created and then diffused from the wall which therefore influences the behaviour of the flow in the wall layer. The experiments of Binder and Kueny (1981) and Tardu and Binder (1993) have put in light that the turbulent field response to the periodic forcing is essentially dependent on the frequency of oscillation, while the amplitude is not a determining parameter. These authors have introduced the dimensionless Stokes length as the relevant parameter; it is defined by $l_s^+ = l_s/l_v$ in the study of turbulent pulsed channel flow, $l_s = \sqrt{2\nu/\omega}$ being the Stokes length and $l_v = \nu/u_\tau$ the viscosity length scale, thus we get $l_s^+ = \sqrt{2u_\tau^2/\nu\omega}$. This length is interpreted as the distance over which the normal gradient is propagated from the wall. The characteristic Strouhal number $\omega^+ = \omega\nu/u_\tau^2$ is directly linked to the dimensionless Stokes length parameter through the relation $\omega^+ = 2/l_s^{+2}$. This means that the higher is the frequency, the tinier is the wall layer affected by the oscillations. In such a case, much of the core flow in the channel is moving in block.

If one considers that the turbulent flow near the wall is dominated by viscous effects up to $z^+ \approx 12$ in wall units, the oscillation wave from the wall will then reach the asymptotic outer value before turbulence can act (Tardu et al., 1994) for frequency regimes that imply $l_s^+ < 12$, and a Stokes behaviour is expected. For $l_s^+ > 12$, the response of the flow will then depart from the Stokes solution.

From numerous parametric studies, Tardu et al. (1994) and Binder et al. (1995) made clear the existence of three frequency regimes: a quasi-steady regime reached for $l_s^+ > 25$, a relaxation regime for $10 < l_s^+ < 13$, in which important amplitude modulations of the turbulence are observed together with phase shift effects, and a high frequency regime for lower values of l_s^+ in which the Stokes solution is reached, but the distribution of velocity departs again from this solution for even lower values $l_s^+ < 8$, the burst-ejection process being modified (Tardu and Binder, 1993).

In the present simulation the superimposed perturbation is produced by a longitudinal sinusoidal mean pressure gradient

$$F_x = -(1 + A_F \sin(\omega t)) \tag{16}$$

We have chosen here $l_s^+ = 12.9$, a value corresponding to an intermediate frequency regime, for which a strong interaction is possible between the scales of the

imposed oscillation and the turbulence itself. The amplitude is chosen to be weak with a value equal to $A_{\tilde{U}_c} = 0.05\ U_c$. This parameter choice corresponds to values used in one of the experiments realised by Binder and Kueny (1981). The numerical simulation has been carried on for the coarse grid defined previously and using the Smagorinsky model and the transport equation model. Results from a computation performed with a finer grid resolution and the Smagorinsky model are also presented to consider the effect of mesh density on

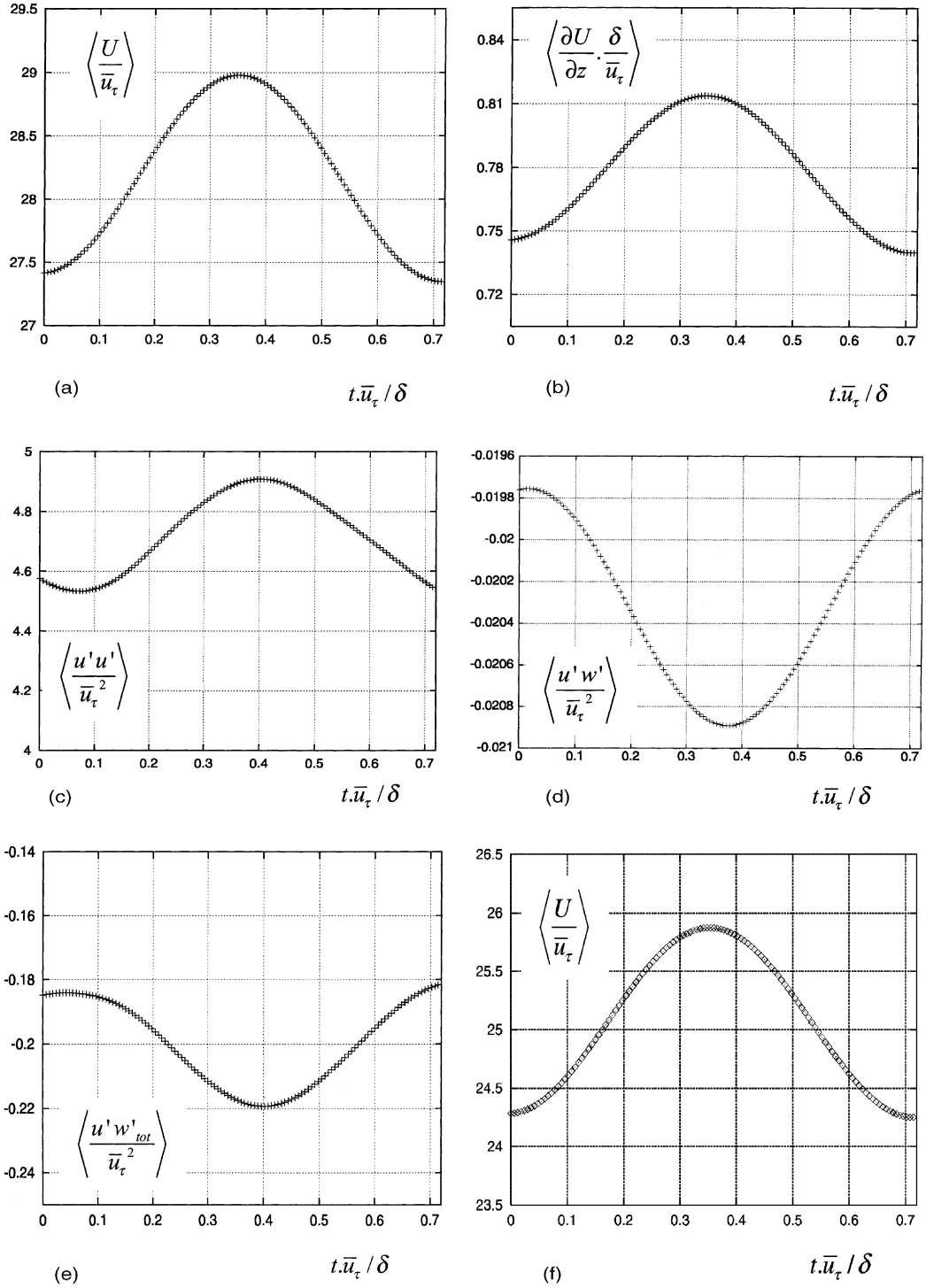

Fig. 8. Phase averages in turbulent pulsed channel flow. (+) (a)–(e) One-equation model ($32 \times 64 \times 62$) and (f)–(j) Smagorinsky model ($32 \times 64 \times 62$): (a,f) longitudinal velocity on the axis ($z = 0$); (b,g) normal component of the velocity gradient at $z^+ = 7.935$; (c,h) longitudinal normal stress at $z^+ = 7.935$; (d,i) explicit turbulent shear stress at $z^+ = 7.935$; (e,j) total turbulent shear stress at $z^+ = 7.935$.

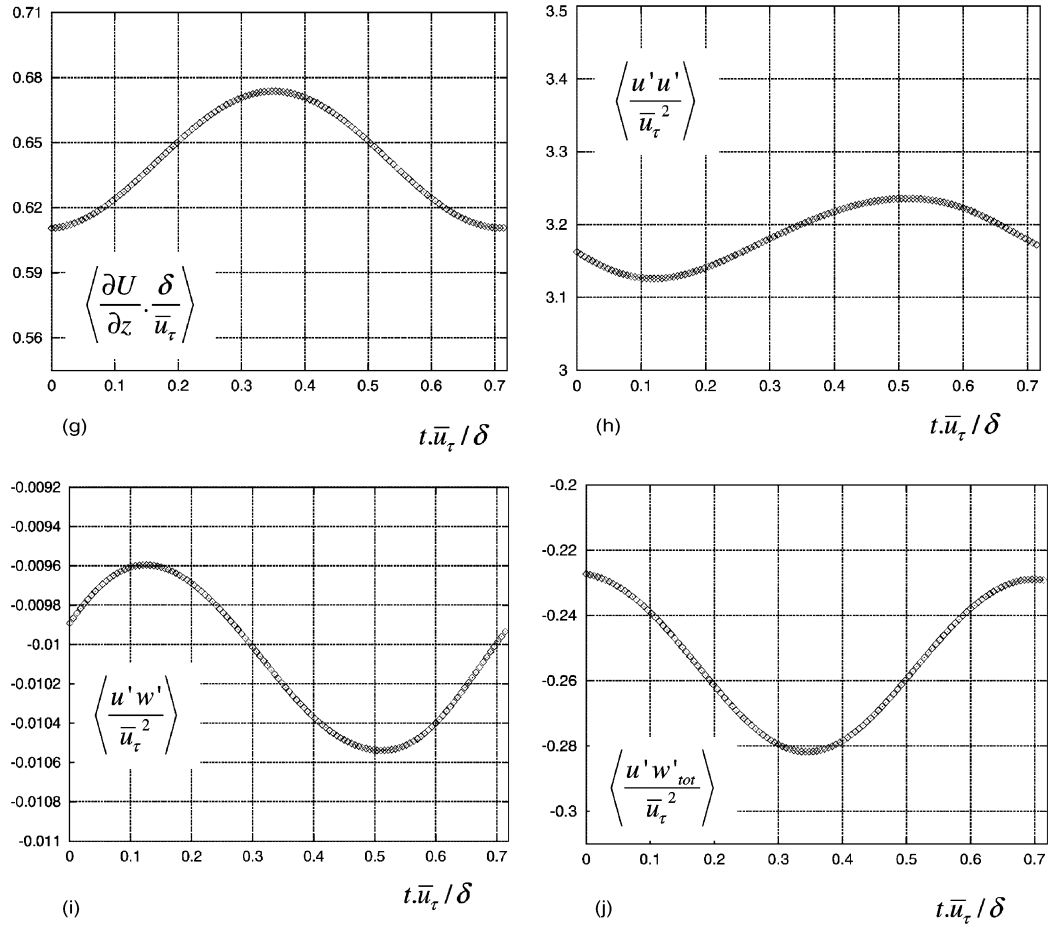

Fig. 8 (*continued*)

the calculated statistical field. The fine grid mesh is identical to the one presented above in the steady channel results section. To gain insight into the flow behaviour, the phase-averaged quantities are analysed in terms of amplitudes and phases of the Fourier modes, the phase average $\{q\} = \langle q \rangle + \tilde{q}$ is decomposed as

$$\{q\} = \langle q \rangle + A_{\tilde{q}} \cos(\omega t + \Phi_{\tilde{q}}) + \sum_{n=2}^{\infty} A_{\tilde{q}n} \cos(n\omega t + \Phi_{\tilde{q}n}) \quad (17)$$

where $A\tilde{q}$ is the amplitude and $\Phi_{\tilde{q}}$ the phase.

4.1. Time averaged flow

In each case, including the Smagorinsky model and the one-equation model calculations, no appreciable difference has been observed between the time mean values obtained in unsteady pulsed channel flow and the time mean values already obtained in steady fully developed channel flow. This absence of any influence coming from the forcing on the time averaged quantities is entirely supported by experimental data (Brereton et al., 1990; Tardu et al., 1994).

4.2. Phase averaged flow

Time evolutions of the phase averages of the longitudinal velocity at the centre channel and of turbulence quantities at a particular distance near the wall are represented on Fig. 8(a–j). These temporal evolutions exhibit time delay between the periodic forcing and the turbulence field modulation. They look very like a sine function, the first Fourier mode being largely dominant. This is confirmed on Fig. 9 showing the level of Fourier modes at a given location for the longitudinal turbulent stresses. Similar results have been obtained at different locations and for others characteristic quantities in the flow. The statistical convergence for phase averaging has been obtained by considering about 24 periods of oscillation in time.

If one examines the amplitudes and phase shifts of the phase averaged velocity, one can observe that the oscillatory forcing affects significantly the wall flow. However, the effect of the forcing appears to be only weakly influenced by the type of model used in the calculation. Both models can predict a velocity response (Fig. 10a and b) in good agreement with the experimental data of Binder and Kueny (1981), Tardu and

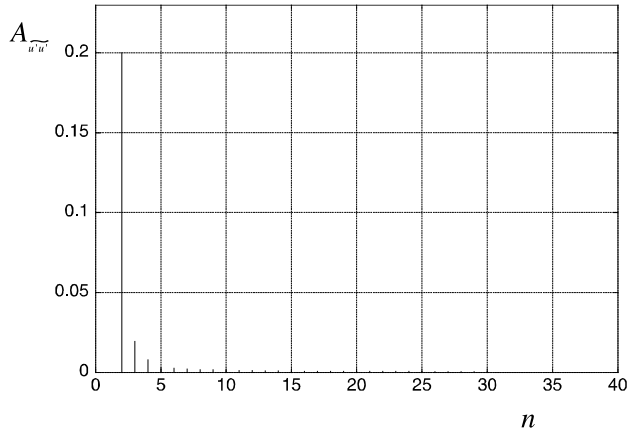

Fig. 9. Amplitude of the primary Fourier mode compared to the secondary Fourier modes for the oscillations of the turbulent longitudinal stresses at $z^+ = 7.935$ distance from the wall, in pulsed channel flow, (+) one-equation model ($32 \times 64 \times 62$).

Binder (1993) and Tardu et al. (1994). The observed modulation is not far from the Stokes solution (see Fig. 10a, dashed lines).

The effect of the pulsation on the velocity field is concentrated near the wall, indeed a steep gradient in this region occurs in the velocity amplitude curve as well as large phase shifts variations. The amplitude and the time scale of the velocity modulation decreases when the distance from the wall is increased. The departure from the Stokes solution is related to the influence of the periodic forcing on the wall turbulence field, the Stokes length parameter in our computation ($l_s^+ = 12.9$) being higher then the critical value ($l_s^+ = 8.1$) for which only the viscous sublayer is affected by the forcing. In Fig. 10a, one can observe that the normal velocity gradient $\partial\overline{U}/\partial z$ induced by the imposed oscillation is diffused up to a $z^+ \approx 50$. ($z_s = 3$) distance from the wall. Considering that this term is the driving force that acts on the turbulent field, this wall zone is expected to be sensitive to the subgrid-scale model. Indeed, if one considers the turbulent field, the behaviour appears clearly different from one model to another. The amplitude of the fundamental mode of the normal longitudinal turbulent stress presented on Fig. 11a reveals that the type of model is strongly determining for the predicted response of the turbulent quantities. In the experiments of Tardu et al. (1994), the amplitude profile is similar to the turbulence intensity profile itself, with a peak region in the region $z^+ = 12$ and a progressive decay afterwards. Fig. 11a shows that qualitatively, only the one-equation transport model is successful in predicting the experimental observations and in particular the experimental peak in amplitude near the wall, whereas the Smagorinsky model provides a totally different amplitude profile, the shape being more rounded, the near wall peak absent and the amplitude decay not well reproduced far from the wall. Due to the particular choice of the axis scaling, the peak observed in the experiments looks as smoothed out. With the aim to put in light the effects of the one-equation model, we have plotted in the inner graph inside Fig. 11a the experimental data along with the one-equation model results scaled with a constant factor 0.42. Note that the maxima predicted by the transport model are in quite good agreement with the measurements and a similar decay with wall distance is also observed. The amplitude profiles $A_{\widetilde{u'u'}}$ normalised by the amplitude of the velocity modulation A_U, represented on Fig. 11b, clearly shows the wall region affected by the forcing: in the measurements, the wall region located up to the distance $z^+ = 20$ strongly interacts with the oscillation, a behaviour which is correctly predicted by the transport equation model. In the case of the Smagorisky model, the near wall region influ-

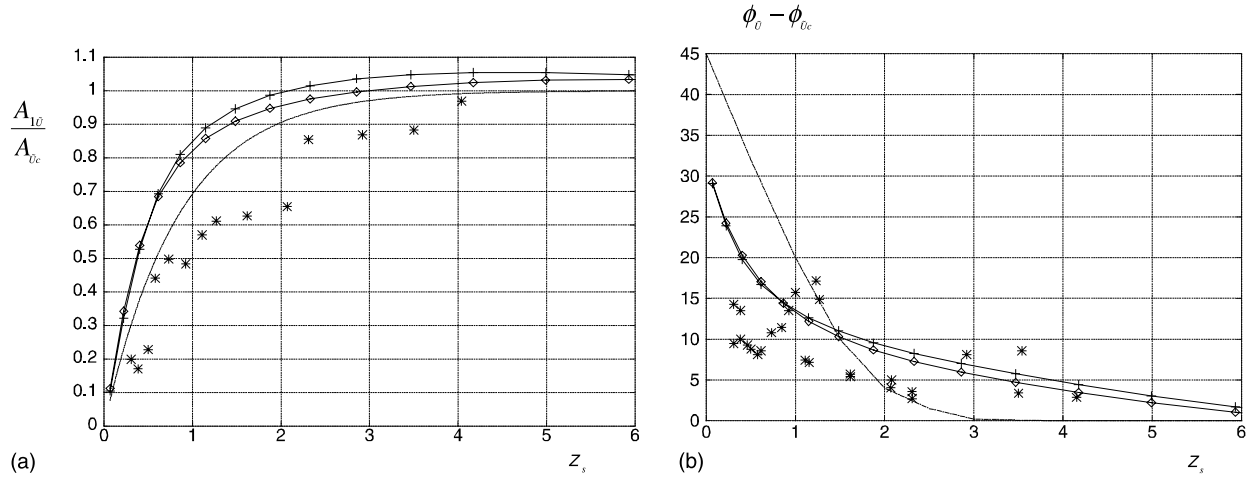

Fig. 10. (a) Amplitude and (b) phase shift of the fundamental mode of the oscillating velocity deviation from axial velocity. (◇) Smagorinsky model ($32 \times 64 \times 62$), (+) one-equation model ($32 \times 64 \times 62$), (∗) Binder and Kueny experiment (1981) $l_s^+ = 12.2$, $a_{\tilde{U}} = 0.05$, $Re = 8500$, (- - -) Stokes solution.

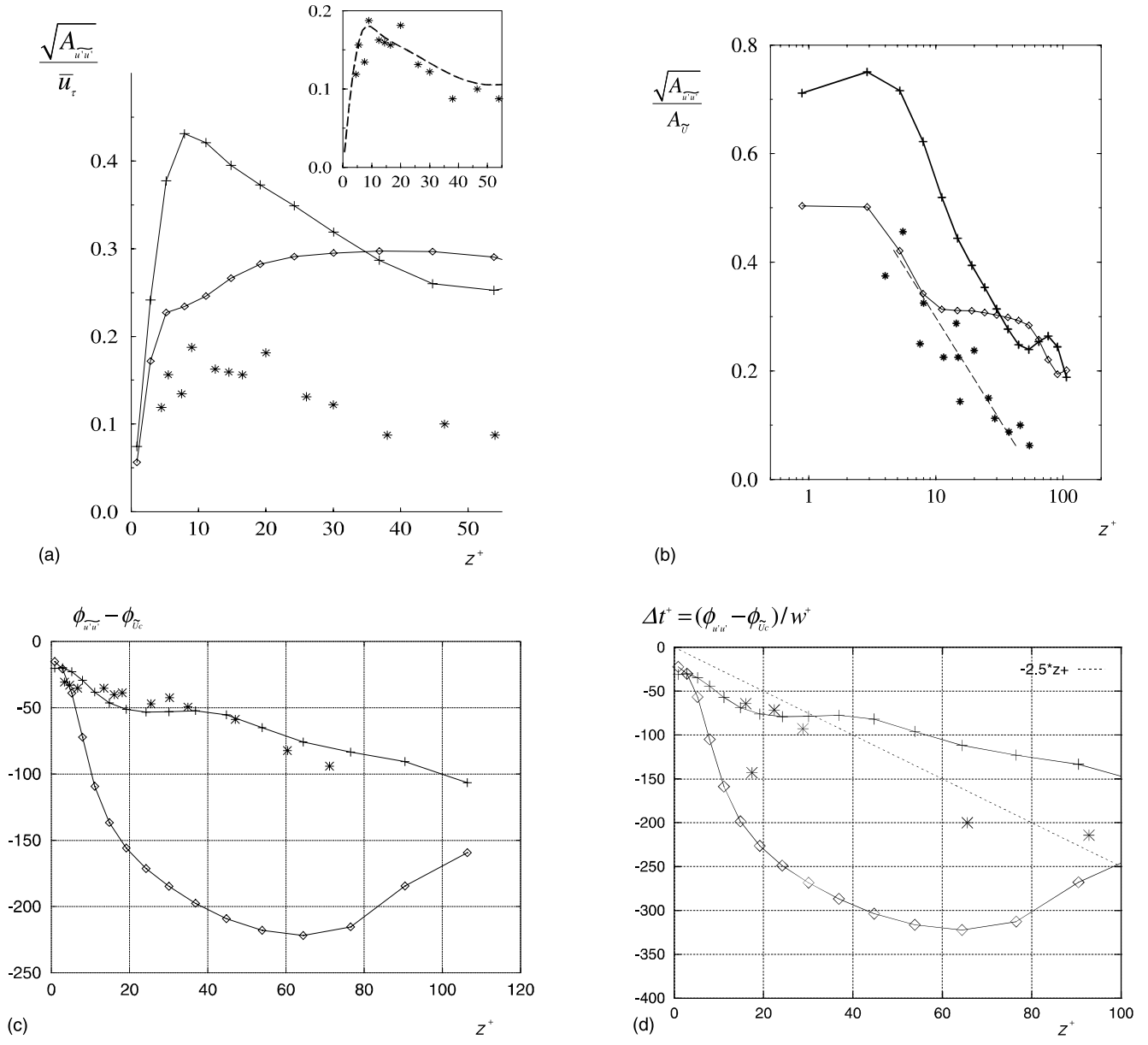

Fig. 11. Amplitude of the fundamental mode of the (a) longitudinal turbulence intensity, (b) normalized longitudinal turbulence intensity ((∗) Binder and Kueny experiment (1981)). (c) Phase shift, (d) dimensionless diffusion time delay of the fundamental mode of the longitudinal turbulence intensity. ((∗) Tardu et al. experiment (1994)). (◇) Smagorinsky model ($32 \times 64 \times 62$), (+) one-equation model ($32 \times 64 \times 62$). $l_s^+ = 12.2$, $a_{\tilde{U}} = 0.05$, $Re = 8500$.

enced by the forcing is thinner (up to $z^+ = 10$) and the amplitude modulation decreases more rapidly. For distances $z^+ > 35$, both models have tendency to produce an identical level of the relative amplitude because of the decreasing effect of the forcing in this flow region. The remaining quantitative discrepancies between the calculated and the measured amplitudes (for velocity and turbulence intensity) are difficult to explain, they may be a consequence of Reynolds number effects, reminding that in the numerical simulation the Reynolds number is 13,800 whereas in the experiment its value is 8600.

As far as phase shifts are concerned, the one-equation model agrees very well with the experimental results, while the Smagorinsky model calculation is far from the measurements (Fig. 11c and d). The phase shift results can also be interpreted in terms of time delay, by using the relation suggested by Tardu et al., 1994:

$$\Delta t^+ = \frac{1}{2}(\phi_{\tilde{u}'u'} - \phi_{\tilde{U}c}) l_s^2 \tag{18}$$

where the phase shifts are calculated in radians. This corresponds to a dimensionless diffusion time giving an order of magnitude of the velocity at which the turbulent

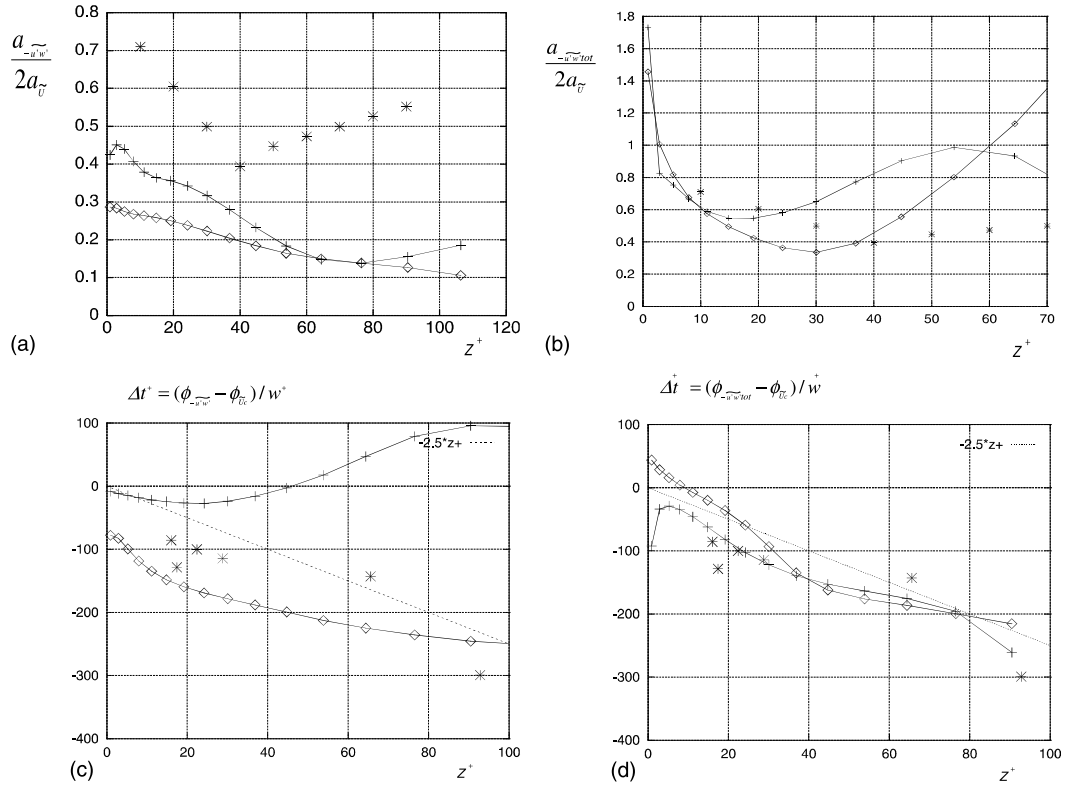

Fig. 12. Relative amplitude of the fundamental mode of the (a) explicit turbulent shear stress, (b) total turbulent shear stress ((∗) Feng et al. (1993)). Dimensionless diffusion time of the fundamental mode of the (c) explicit turbulent shear stress modulation, (d) total turbulent shear stress modulation ((∗) Binder et al. experiment (1995)). (◇) Smagorinsky model ($32 \times 64 \times 62$), (+) one-equation model ($32 \times 64 \times 62$), $l_s^+ = 12$, $a_{\tilde{U}} = 0.2$, $Re = 8500$.

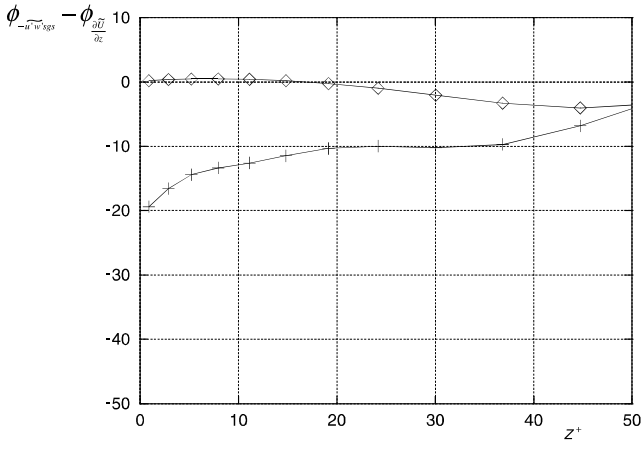

Fig. 13. Difference in phase shift between the subgrid-scale turbulent shear stress modulation and the normal velocity gradient modulation versus z^+, (◇) Smagorinsky model ($32 \times 64 \times 62$), (+) one-equation model ($32 \times 64 \times 62$).

intensity modulation is propagated away from the wall. In the experiments, it has been shown that in the range $8.1 < l_s^+ < 34$, the variations of the time delay versus distance from the wall, verify a linear decay such that $dz^+/d(\Delta t^+) \approx 0.4$ for $z^+ > 30$. Recast in terms of phase lag, this linear law becomes $d(\phi_{u'_i u'} - \phi_{\tilde{U}c})/dz^+ = 2.5\omega^+$ and also better fits the transport model predictions (see Fig. 14).

Further insight is given now by considering the terms involved in the production of the turbulence kinetic energy $P = \langle P \rangle + \tilde{P}$ with

$$\begin{aligned} \langle P \rangle &= -\langle u'w' \rangle \frac{\partial \langle U \rangle}{\partial z} \\ \tilde{P} &= -\langle u'w' \rangle \frac{\partial \tilde{U}}{\partial z} - \widetilde{u'w'} \frac{\partial \langle U \rangle}{\partial z} - \widetilde{u'w'} \frac{\partial \tilde{U}}{\partial z} \end{aligned} \tag{19}$$

In the latter expression of $\tilde{P}$, the third term is negligible compared to the first two terms. Previous results suggested that the time mean velocity gradient, the modulation of the velocity gradient and the time mean turbulent shear stress are all of them only weakly dependent of the subgrid-scale model. So, the model dependence observed on the modulation of the turbulence intensity mainly comes from the contribution of the modulation of turbulent shear stress. The total oscillating turbulent shear stress can be decomposed as follows:

$$\widetilde{u'w'}_{\text{tot}} = \widetilde{u'w'}_{\text{exp}} + \widetilde{u'w'}_{\text{imp}} \tag{20}$$

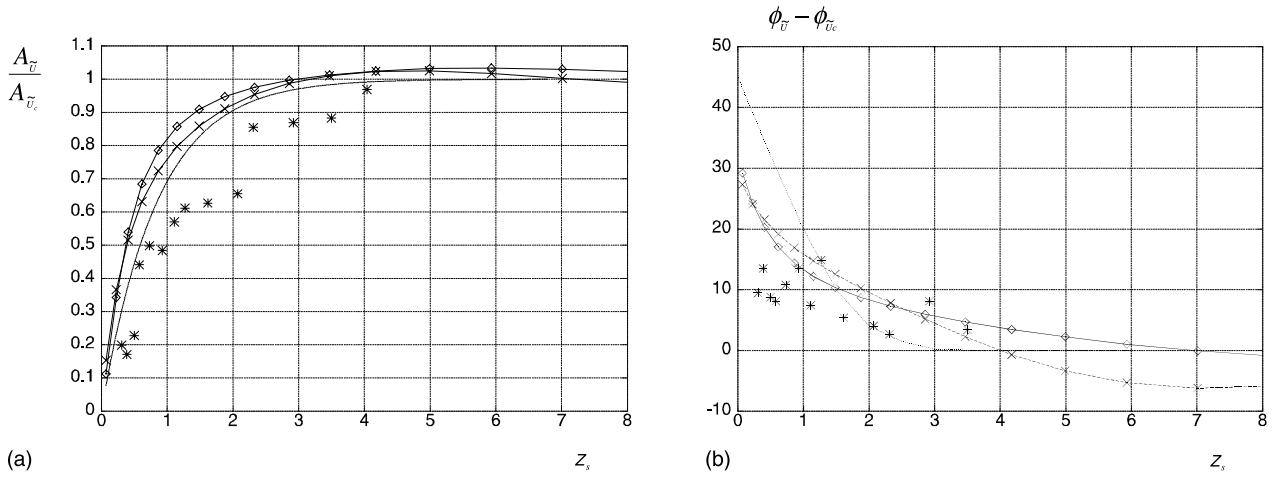

Fig. 14. Fundamental mode of the oscillating velocity deviation from axial velocity (a) amplitude and (b) phase shift. (◇) Smagorinsky model ($32 \times 64 \times 62$), (×) Smagorinsky model ($256 \times 128 \times 62$), (∗) Binder and Kueny experiment (1981), $l_s^+ = 12.2$, $a_{\tilde{U}} = 0.05$, $Re = 8500$, (- - -) Stokes solution.

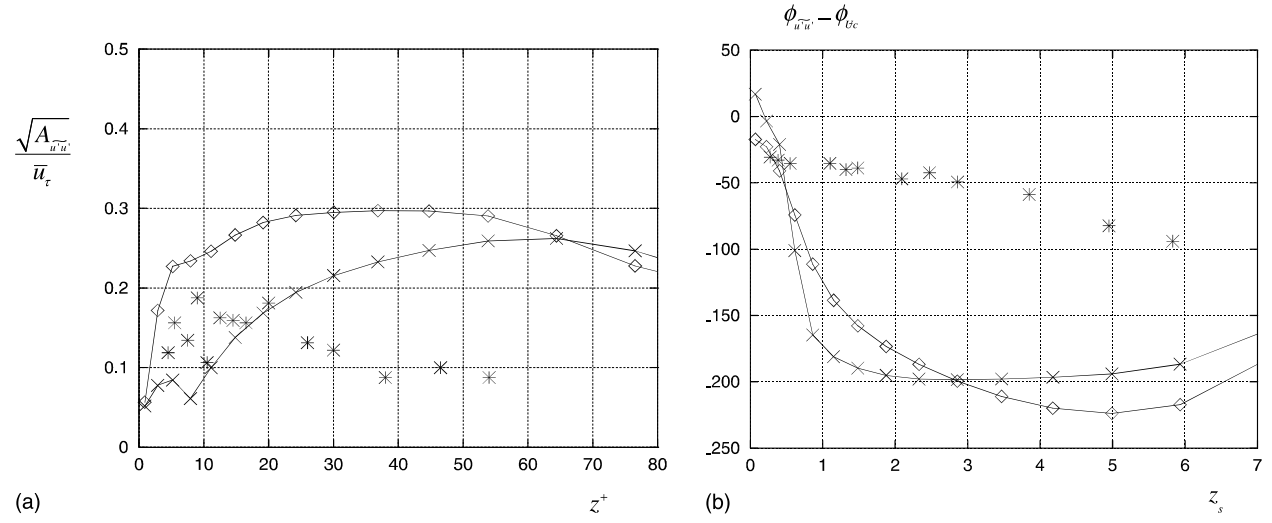

Fig. 15. Fundamental mode of the longitudinal turbulence intensity (a) amplitude and (b) phase shift. (◇) Smagorinsky model ($32 \times 64 \times 62$), (×) Smagorinsky model ($256 \times 128 \times 62$), (∗) Binder and Kueny experiment (1981), $l_s^+ = 12.2$, $a_{\tilde{U}} = 0.05$, $Re = 8500$.

In Fig. 12a and b are plotted the amplitude for the explicit part and for the total turbulent shear stress. The available experimental data (Tardu et al., 1994) used to compare the behaviour of the turbulent shear stress modulation correspond to the same Stokes length parameter $l_s^+ = 12.5$ but to a different amplitude of the forcing velocity $\tilde{a}_c = 0.2$. However, recalling that according to the experimental results the amplitude of the forcing is not the leading parameter for pulsed channel flow but that the relevant parameter is indeed the Stokes length, the measurements realised for the relative amplitude $\tilde{a}_c = 0.2$. can be exploited for our analysis. Compared to the experiment, the amplitude profile shape of the total turbulent shear stress $\widetilde{u'w'}_{\text{tot}}$ and its resolved part $\widetilde{u'w'}_{\text{exp}}$ are in good agreement. As for the longitudinal turbulence intensity, the relative amplitude of the shear stress modulation decreases away from the wall. The comparison of the total shear stress amplitude to its explicit part shows the importance of the modelled subgrid contribution $\widetilde{u'w'}_{\text{imp}}$. Model dependent effects are clearly apparent on the explicit turbulent shear stress amplitude in the very near wall region. Indeed, for distances such that $0 < z^+ < 20$, the amplitude of the resolved turbulent stress in the one-equation case presents higher values than in the Smagorinsky case.

Similar observations can be made for the distribution of the time delay (Fig. 12c and d) which is the dimensionless diffusion time versus the wall distance for $\widetilde{u'w'}_{\text{tot}}$

and $\widetilde{u'w'}_{\exp}$. In the case of the Smagorinsky model and the one-equation model, the time delay obtained for the resolved scales and for the total shear contribution are clearly different. In the near wall region, the two models can give differences between the values of the dimensionless diffusion time that can reach up to 140 for the total shear stress. Compared to the measurements, the one-equation model provide better predictions (Fig. 12d). The temporal response of the subgrid-scale turbulent viscosity to the velocity gradient oscillation (Fig. 13) reveals that some history effects are clearly accounted for by the transport model.

Because of the mesh resolution effects already mentioned, an additional numerical simulation has been carried on with a finer grid resolution (identical to the one used in the steady case) and the Smagorinsky model. Comparison between the computations of the oscillatory flow performed with the coarse and the fine grid meshes and the Smagorinsky model are presented on Figs. 14 and 15a and b. The two calculations lead to similar results concerning the velocity and turbulent fields quantities. The finer description of the longitudinal and streamwise vortices due to the refinement in x and y-directions did not influence significantly the turbulent field as it has been the case in the steady flow. Obviously, one has to keep in mind that, irrespective to the type of model used, going to a finer grid resolution in all the three spatial directions must provide a better agreement because the calculation will be closer to a DNS. However, such calculations are costly in computer time and therefore the transport equation model appears to be an efficient alternative in simulations using a coarse mesh.

5. Concluding remarks

The results presented in this paper have shown an encouraging first step in the simulation of unsteady turbulent flows. For such flows, the unresolved turbulent scales exhibit a determining role and thus the subgrid-scale model must take into account the history effects. This is not possible at all with the Smagorinsky model which is based on an instantaneous adjustment of the implicit turbulent shear stress with the explicit deformation tensor. The transport equation model proved to be an efficient method in the development of models that bridge the LES approach and the RANS approach.

Future work would probably have to concentrate on the assumption of the characteristic length for dissipation, which is directly linked to the filter size. Indeed, when very large eddy simulations in which the cut-off can be located before the spectral inertial range, this assumption will have to be revised (Dejoan and Schiestel, 1999). However, the various applications carried on for unsteady turbulent flows (Dejoan et al., 1997; Dejoan, 1998) have put in light the interesting potentials of the present method for the simulation of turbulent flows undergoing departures from equilibrium due to unsteadiness in the mean. In the turbulent pulsed channel flow, the one-equation model gives a far better determination of the phase-shifts linked to the lag effects produced by unsteadiness.

Acknowledgements

The calculations have been carried on the CRAY C98 supercomputers at the IDRIS computer centre in Paris, which is gratefully acknowledged.

Appendix A. Determination of numerical constants in the one-equation model

The determination of the numerical constants in the one-equation transport model is made by reference to the zero pressure gradient turbulent boundary layer.

In the fully turbulent zone, the turbulent viscosity and the dissipation rate take the form

$$\nu_{\mathrm{sgs}} = C_{\nu\mathrm{sgs}} l_{\mathrm{sgs}} k_{\mathrm{sgs}}^{1/2} \quad \text{and} \quad \varepsilon_{\mathrm{sgs}} = C_{\varepsilon\mathrm{sgs}} \frac{k_{\mathrm{sgs}}^{3/2}}{l_{\mathrm{sgs}}} \tag{A.1}$$

The production term is given by

$$\mathscr{P} = 2\nu_{\mathrm{sgs}} \overline{S}_{ij} \overline{S}_{ij} \tag{A.2}$$

The equilibrium hypothesis implies

$$k_{\mathrm{sgs}} = 2\overline{S}_{ij}\overline{S}_{ij} \frac{C_{\nu\mathrm{sgs}} l_{\mathrm{sgs}}^2}{C_{\varepsilon\mathrm{sgs}}} \tag{A.3}$$

From the modelled turbulent viscosity given by (A.1), one can deduce the value of kinetic energy

$$k_{\mathrm{sgs}} = \left(\frac{\nu_{\mathrm{sgs}}}{C_{\nu\mathrm{sgs}} l_{\mathrm{sgs}}} \right)^2 \tag{A.4}$$

and from the two previous equations, it comes

$$\nu_{\mathrm{sgs}} = C_{\nu\mathrm{sgs}} \left(\frac{C_{\nu\mathrm{sgs}}}{C_{\varepsilon\mathrm{sgs}}} \right)^{1/2} l_{\mathrm{sgs}}^2 (2\overline{S}_{ij}\overline{S}_{ij})^{1/2} \tag{A.5}$$

Comparing to the Smagorinsky model $\nu_{\mathrm{sgs}} = (C_s l)^2 \times (2\overline{S}_{ij}\overline{S}_{ij})^{1/2}$ a first relation is obtained between the coefficients

$$C_{\nu\mathrm{sgs}} \left(\frac{C_{\nu sgs}}{C_{\varepsilon\mathrm{sgs}}} \right)^{1/2} = C_s^2 \tag{A.6}$$

When the upper limit of the mixing length is reached

$$\mathscr{P} = \nu_{\mathrm{sgs}} \left| \frac{\partial \overline{U}}{\partial z} \right|^2 = \varepsilon_{\mathrm{sgs}} \tag{A.7}$$

and the following relation holds

$$C_s^2 l_{\mathrm{sgs}}^2 \left| \frac{\partial \overline{U}}{\partial z} \right|^3 = C_{\varepsilon\mathrm{sgs}} \frac{k_{\mathrm{sgs}}^{3/2}}{l_{\mathrm{sgs}}} \quad \text{or} \quad \frac{u_\tau^3}{\kappa z} = C_s C_{\varepsilon\mathrm{sgs}} \frac{k_{\mathrm{sgs}}^{3/2}}{\kappa z}$$

and then a second relation is obtained

$$\left(\frac{u_\tau^2}{k_{sgs}}\right)^{3/2} = C_s C_{\varepsilon sgs} \tag{A.8}$$

where the value of u_τ^2/k ($k_{sgs} \to k$) is estimated by 0.3.

In the viscous sublayer, the turbulent Reynolds number is low and when $R_{sgs} \to 0$, the subgrid viscosity is equivalent to

$$\nu_{sgs} = C_{\nu sgs} l_{sgs} k_{sgs}^{1/2} A_{\nu sgs} R_{sgs} = \frac{C_{\nu sgs} l_{sgs}^2 A_{\nu sgs} k_{sgs}}{\nu} \tag{A.9}$$

and the dissipation can be approximated by

$$\varepsilon_{sgs} = \frac{2\nu k_{sgs}}{l_{sgs}^2} + \frac{C_{\varepsilon sgs} A_{\nu sgs} k_{sgs}^2}{\nu} \to \frac{2\nu k_{sgs}}{l_{sgs}^2} \tag{A.10}$$

Very near the wall the dissipation and diffusion terms are in balance, so

$$\mathscr{D}_{sgs} = \frac{2\nu k_{sgs}}{l_{sgs}^2} \tag{A.11}$$

In the viscous sublayer, the approximate balance is

$$2\nu_{sgs}\overline{S}_{ij}\overline{S}_{ij} + \mathscr{D}_{sgs} = \varepsilon_{sgs} \tag{A.12}$$

Using the relations (A.9) to (A.11), one can deduce from (A.12) a relation for kinetic energy which is identical to (A.3). This relation once reported into (A.9) gives

$$\nu_{sgs} = \frac{C_{\nu sgs}^2 l_{sgs}^4 A_{\nu sgs}}{\nu C_{\varepsilon sgs}} (2\overline{S}_{ij}\overline{S}_{ij}) \tag{A.13}$$

Compared to (5b), a new relation is obtained between the numerical constants

$$A_{\nu sgs} = \frac{C_{\varepsilon sgs} C_S^4}{27\kappa C_{\varepsilon sgs}^2} \tag{A.14}$$

Using $C_s = 0.2$, the following numerical values are obtained

$$C_{\nu sgs} = 0.116, \quad C_{\varepsilon sgs} = 0.85, \quad A_{\nu sgs} = 0.229$$

Also the pseudo Prandtl number for turbulent diffusion is taken to be $\sigma_{sgs} = 1$, like in the full statistical model.

References

Binder, G., Kueny, J.L., 1981. Measurements of the periodic oscillations near the wall in unsteady turbulent channel flow. In: Michel, R., Cousteix, J., Houdeville, R. (Eds.), Unsteady Turbulent Shear Flows, IUTAM Symposium. Springer, Berlin, pp. 100–109.

Binder, G., Tardu, S., Vezin, P., 1995. Cycle modulation of Reynolds stresses and length scales in pulsed channel flow. Proc. Roy. Soc. London A 451, 121–139.

Brereton, G.J., Reynolds, W.C., Jayaraman, R., 1990. Response of a turbulent boundary layer to sinusoidal free-stream unsteadiness. J. Fluid Mech. 221, 331–359.

Comte-Bellot, G., 1965. Ecoulement turbulent entre deux parois parallèles. Publication Scientifique et Technique du Ministère de l'Armée de l'Air, 419.

Deardorff, J.W., 1973. The use of subgrid transport equations in a three-dimensional model of atmospheric turbulence. J. Fluid Engng. ASME 95, 429–438.

Dejoan, A., 1998. Simulation de grandes échelles turbulentes en écoulement de canal plan soumis à des perturbations instationnaires. Thèse de Doctorat Université d'Aix-Marseille II.

Dejoan, A., Schiestel, R., Simulation de grandes échelles en écoulement turbulent soumis à des perturbations instationnaires, Actes du 14ème Congrès Français de Mécanique, AUM, Toulouse, Communication réf. 453, 30 août-3 September 1999.

Dejoan, A., Vedy, E., Schiestel, R., 1997. Large eddy simulation of perturbed turbulent wall flows, In: Proceedings of 11th Symposium On Turbulent Shear Flows, Grenoble, France, vol. 3, pp. 30.25–30.30.

Feng, M., Tardu, S., Binder, G., 1993. Inner region of unsteady channel flow. In: So, R.M.C., Speziale, C.G., Launder, B.E. (Eds.), Near wall turbulent flows. Elsevier, New York, pp. 457–466.

Germano, M., Piomelli, U., Moin, P., Cabot, W.H., 1991. A dynamic subgrid-scale eddy viscosity model. Phys. Fluid A 3 (7), 1760–1765.

Hanjalic, K., Stosic, N., 1983. Hysteresis of turbulent stresses in wall flows subjected to periodic disturbances. In: Bradbury, L.J.S. et al. (Eds.), Proceedings of the Symposium on Turbulent Shear Flows, vol. 4, pp. 287–300.

Hassid, S., Poreh, M., 1975. A turbulent energy model for flows with drag reduction. J. Fluid. Engng. 75-FE-H.

Horiuti, K., Yoshizawa, A., 1986. Large-eddy simulation of turbulent channel flow by 1-equation model. In: Schumann, U., Friedrich, R. (Eds.), Notes on Numerical Fluid Mechanics, Direct and Large-eddy Simulation of Turbulence, Proceedings of EUROMECH Coll. No. 199, München, 1985, vol. 15. Vieweg Verlag, pp. 119–134.

Hussain, A.K.M.F., Reynolds, W.C., 1975. Measurements in fully developed turbulent channel flow. J. Fluid Engng. Trans. ASME I 97, 568–578.

Kreplin, H.P., Eckelman, H., 1979. Behaviour of the three fluctuating velocity components in the wall region of a turbulent channel flow. Phys. Fluid 22 (7), 1233–1239.

Kwak, D., Reynolds, W.C., Ferziger, J.H., 1975. Three-dimensional time-dependent computation of turbulent flows. Dept. of Mech. Engng. Stanford Univ. Calif. Report TF-5.

Metais, O., Lesieur, M., 1992. Spectral large-eddy simulation of isotropic and stably stratified turbulence. J. Fluid Mech. 125, 475–503.

Moin, P., Kim, J., 1982. Numerical investigation of turbulent channel flow. J. Fluid Mech. 118, 341–377.

Piomelli, U., Moin, P., Ferziger, J.H., 1988. Model consistency in large-eddy simulation of turbulent channel flow. Phys. Fluid 31 (7), 1884–1891.

Reynolds, W.C., Hussain, A.K.M.F., 1972. The mechanics of an organized wave in turbulent shear flow. Part 3: theoretical models and comparisons with experiments. J. Fluid Mech. 54, 263–288.

Schiestel, R., Viazzo, S., 1995. A Hermitian–Fourier numerical method for solving the incompressible Navier–Stokes equations. Comput. Fluid. 24 (6), 739–752.

Schumann, U., 1975. Subgrid-scale model for finite difference simulations of turbulent flows in plane channels and annuli. J. Comp. Phys. 18, 367–404.

Tardu, S., Binder, G., 1993. Wall shear stress modulation in an unsteady turbulent channel flow with hight imposed frequencies. Phys. Fluid. A 5 (8), 2028–2037.

Tardu, S., Binder, G., Blackwelder, R., 1994. Turbulent channel flow with large amplitude velocity oscillations. J. Fluid Mech. 267, 109–151.

Viazzo, S., 1993. Simulation de grandes structures turbulentes en canal plan et application à l'étude du champ de pression pariétale. Thèse Université Aix-Marseille II.

Viazzo, S., Schiestel, R., 1995. Simulations des grandes échelles turbulentes en canal à l'aide d'un schéma hermitien. Comptes Rendus de l'Académie des Sciences 321 (série II b), 225–232.